This document is the Accepted Manuscript version of a Published Work that appeared in final form in **Journal of Physical Chemistry C**, **copyright 2019 American Chemical Society** after peer review and technical editing by the publisher. To access the final edited and published work see https://doi.org/10.1021/acs.jpcc.9b03621
Postprint of: Staniszewska M., Kupfer S., Guthmuller J., Effect of the Catalytic Center on the Electron Transfer Dynamics in Hydrogen-Evolving Ruthenium-Based Photocatalysts Investigated by Theoretical Calculations, Journal of Physical Chemistry C Vol. 123, Iss. 26 (2019), pp.16003-16013

Effect of the Catalytic Center on the Electron Transfer Dynamics in Hydrogen-Evolving Ruthenium-Based Photocatalysts Investigated by Theoretical Calculations

Magdalena Staniszewska[1], Stephan Kupfer*[2] and Julien Guthmuller*[1]

[1]Faculty of Applied Physics and Mathematics, Gdańsk University of Technology, Narutowicza 11/12, 80233 Gdańsk, Poland

[2]Institute of Physical Chemistry and Abbe Center of Photonics, Friedrich Schiller University Jena, Helmholtzweg 4, 07743 Jena, Germany

* julien.guthmuller@pg.edu.pl ; stephan.kupfer@uni-jena.de

Abstract

The light-induced relaxation pathways in the molecular photocatalyst $[(tbbpy)_2Ru(tpphz)PtCl_2]^{2+}$ are investigated with time-dependent density functional theory calculations together with the Marcus theory of electron transfer (ET). The calculations show that metal (Ru) to ligand (tpphz) charge transfer (MLCT) triplet states are populated following an excitation in the longer wavelength range of the absorption spectrum, but that an ET toward the catalytic center ($PtCl_2$) from these states is thermodynamically unfavorable, implying that charge separation can only occur via higher energy states in this system. Moreover, low-lying Pt-centered states can be populated and the calculations predict that they can form an excited state equilibrium with MLCT states localized on the tpphz ligand. A comparison with previously reported results[1] for the photocatalyst $[(tbbpy)_2Ru(tpphz)PdCl_2]^{2+}$, based on a $PdCl_2$ catalytic center, is provided in order to decipher the effect of the catalytic center on their respective photochemistry.

1. Introduction

Nowadays, motivated by the need of sustainable sources of energy, extensive research efforts are conducted to design new devices for the conversion of solar energy into so-called solar fuels. One approach consists of using photocatalytic systems that split the water molecules into molecular hydrogen (to be employed as fuel) and oxygen. To this aim, several hydrogen-evolving molecular photocatalysts were proposed[2,3,4,5,6,7,8,9,10], which are typically composed of three molecular components, namely (i) a photosensitizer, where the light absorption occurs, (ii) a bridging ligand, that stores electron(s) and mediates the electron transfer (ET), and (iii) a catalytic center, where the molecular hydrogen is formed. The improvement of the catalytic efficiency in these systems requires a precise understanding of the photochemical mechanisms as well as of the interplay between the three components. Such knowledge can in principle be obtained by theoretical methods, which allow the prediction of the molecular properties related to light absorption, of the photo-induced ET as well as how these processes are impacted by structural modifications of the photocatalyst.

The goal of this work is to investigate the molecular photocatalyst $[(tbbpy)_2Ru(tpphz)PtCl_2]^{2+}$ (tbbpy=4,4'-di-*tert*-butyl-2,2'-bipyridine, tpphz=tetrapyrido[3,2-a:2',3'-c:3'''-h:2''',3'''-j]phenazine) (Figure 1), denoted $RuPtCl_2$, and to compare its properties to the previously studied photocatalyst[1] $[(tbbpy)_2Ru(tpphz)PdCl_2]^{2+}$ (denoted as $RuPdCl_2$), in order to estimate the effect of the catalytic center ($PtCl_2$ or $PdCl_2$) on the ET properties. The tpphz-based photocatalysts were proposed by the group of Sven Rau starting in 2006 with $RuPdCl_2$[2]. In the following years they were the focus of several studies[11,12,13,14,15,16,17] aiming to understand their photochemistry and to optimize their photocatalytic activity by for example modification of the catalytic center[18,8,9]. In $RuPtCl_2$, $RuPdCl_2$ and in related systems the catalytic center must be photoreduced twice to produce molecular hydrogen[2,8,9,16,19,20,18,11]. These previous studies have shown that the first photo-induced ET from the photosensitizer toward the catalytic center proceeds in the following sequence: 1) light absorption leads to the population of singlet metal-to-ligand

MOST WIEDZY Downloaded from mostwiedzy.pl

charge-transfer (MLCT) states localized on both the tpphz and tbbpy ligands, 2) ultrafast intersystem crossing (ISC) and excited state relaxation processes populate triplet MLCT state(s) (in the vicinity of the initially excited singlet MLCT states) localized predominantly on the tpphz bridging ligand, and 3) ET leads to the reduction of the catalytic center and consequently to the formation of a charge-separated (CS) species. Moreover, it was proposed that the charge separation process in $RuPdCl_2$ (step 3 in the previous sequence) involves a partial degradation of the catalytic center, i.e., the dissociation of a Cl^- ion[2,11]. Additionally, in a former study[8] investigating the catalysis of $RuPdCl_2$ and $RuPtCl_2$ it was found that $RuPdCl_2$ is subject to an alteration of the catalytic center resulting in the formation of metal colloids during catalysis. On the contrary, the $RuPtCl_2$ and the $RuPtI_2$ (based on a PtI_2 catalytic center) photocatalysts are stable during the catalysis[9], which indicates a different catalytic mechanism that does not involve formation of colloids. The modification of the catalytic center also affects the turnover number (TON) for hydrogen generation. Indeed, a small TON of 7 was reported[8] for $RuPtCl_2$, whereas larger TON of 238 and 276 were obtained[9,19] for $RuPdCl_2$ and $RuPtI_2$, respectively. Recently, the light-induced relaxation pathways populated upon excitation in the longer wavelength range of the $RuPdCl_2$ absorption spectrum were investigated theoretically using density functional theory (DFT), time-dependent DFT (TD-DFT) and the semi-classical Marcus theory.[1] These calculations predict that low-lying Pd-centered states are efficiently populated and it was proposed that these states lead to the dissociation of Cl^- and are consequently responsible for the experimentally observed (partial) degradation of the catalytic center. However, according to experimental studies[8,9] such degradation does not occur in $RuPtCl_2$, which points to differences in the excited state relaxation cascades between $RuPdCl_2$ and $RuPtCl_2$. Preliminary results concerning the triplet excited states energies have shown that CS states and Pd/Pt-centered states are destabilized by about 0.5-1.0 eV when going from $RuPdCl_2$ to $RuPtCl_2$, which is expected to influence the ET processes[17]. Therefore, it is the aim of this contribution to provide a detailed theoretical investigation of the excited state properties (including the effects of structural relaxation on the relevant excited states) and of the

MOST WIEDZY Downloaded from mostwiedzy.pl

light-driven ET processes in $RuPtCl_2$ using a similar protocol as employed for $RuPdCl_2$. In this way, the comparison of both systems will shed light on the differences between their respective photochemistry.

The paper is organized as follows: section 2 presents the theoretical methods and the methodology used to estimate the ET rates. Section 3.1 describes the singlet and triplet excited state properties at the ground state geometry. Sections 3.2 and 3.3 provide an in-depth investigation of the electron and energy transfer processes in $RuPtCl_2$ and a comparison with $RuPdCl_2$. Finally, a conclusion is provided in section 4.

MOST WIEDZY Downloaded from mostwiedzy.pl

2. Theoretical methods

2.1 Quantum chemistry calculations

All quantum chemical calculations were performed with the Gaussian 09 program,[21] which provided the structural and electronic properties of the $RuPtCl_2$ complex. To reduce the computational cost of the calculations without affecting the properties, the structure of the complex was simplified by replacing the *tert*-butyl groups by methyl groups (Figure 1). The equilibrium geometry of the singlet ground state (S_0) was obtained by means of DFT by using the B3LYP exchange-correlation (XC) functional.[22,23] The calculation of the harmonic vibrational frequencies confirmed that the optimized structure corresponds to a minimum on the potential energy surface. The 28-electron and 60-electron relativistic effective core potentials MWB[24] were used with their basis sets for the ruthenium and platinum atoms, respectively. The 6-31G(d) basis set[25] was employed for the main-group elements. Vertical excitation energies, oscillator strengths, and electronic characters of the 100 lowest singlet and 80 lowest triplet excited states were calculated with TD-DFT. These calculations were performed at the S_0 geometry by using the same XC functional, basis sets, and core potentials. Additionally, the geometries of several excited states involved in the light-driven ET dynamics were optimized with TD-DFT. This computational protocol was already successfully applied to simulate the UV-vis absorption and resonance Raman spectra, the spectro-electrochemistry properties and the ET dynamics in structurally related transition metal complexes.[13,14,15,26,1,17] In particular, it has shown to provide a balanced description of the ground and excited states properties for electronic states of different nature. The effects of the interaction with a solvent (i.e., acetonitrile, ε = 35.688, n = 1.344) were taken into account for the ground state and the excited states properties by the integral equation formalism of the polarizable continuum model[27] (IEFPCM). The non-equilibrium procedure of solvation was used for the calculation of the vertical singlet-singlet and singlet-triplet excitation energies at the different geometries, which is well-adapted for processes where only the fast reorganization of the electronic

MOST WIEDZY Downloaded from mostwiedzy.pl

distribution of the solvent is important. In contrast, the equilibrium procedure of solvation was applied for the excited state geometry optimizations.

2.2 Electron-transfer kinetics

To access the non-adiabatic photo-induced ET processes in $RuPtCl_2$ the semi-classical Marcus theory was applied.[28,29] In Marcus theory, such ET dynamics proceed along the parabolic diabatic potential energy curves (PECs) of the electron donor state (D) and the acceptor state (A) along the reaction coordinate R_{ET}. Structural distortion within the donor state – induced by thermal fluctuations of the surrounding bath (e.g., the solvent) – may provide sufficient electronic coupling between D and A to allow the ET to occur. The rate equation for such ET process is then given by Equation (1),

$$k_{\mathrm{ET}} = \frac{2\pi}{\hbar}\left|V_{\mathrm{D/A,\,max}}\right|^2 (4\pi\lambda k_{\mathrm{B}}T)^{-1/2} \exp\left(-\frac{(\Delta G+\lambda)^2}{4\lambda k_{\mathrm{B}}T}\right) \quad (1)$$

in which $V_{D/A,max}$ corresponds to the maximum potential coupling matrix element between the electron donor state D and the electron acceptor state A at the crossing point of the diabatic PECs, λ is the reorganization energy, ΔG is the driving force of the ET (Gibbs free energy) and T (295 K) is the temperature. In case of $RuPtCl_2$ all investigated donor and acceptor states were of triplet multiplicity. The ET kinetics for the different pairs of D/A states were assessed along linear-interpolated Cartesian coordinates (LICCs) connecting the optimized equilibrium structures of the donor and acceptor states. The diabatic PECs for D and A were constructed along these LICCs (denoted R_{ET}) by means of TD-DFT single-point calculations.

In order to calculate the potential coupling matrix elements ($V_{D/A}(R_{ET})$) between D and A along R_{ET}, a straightforward diabatization of the PECs was achieved by manually following the electronic transitions for each state of interest along the LICC. Then, the diabatic PECs were fitted by a quadratic polynomial, whereas the adiabatic PECs were obtained by a cubic (B-)spline interpolation along R_{ET} by using a total number of 100 grid points. The potential couplings $V_{D/A}$ are

MOST WIEDZY Downloaded from mostwiedzy.pl

then retrieved by an unitary transformation of the adiabatic potential matrix V_i^{ad} for each R_{ET} [Eq. (2)].

$$\begin{pmatrix} V_D & V_{D/A} \\ V_{D/A} & V_A \end{pmatrix} = U^{+} \begin{pmatrix} V_1^{ad} & 0 \\ 0 & V_2^{ad} \end{pmatrix} U \tag{2}$$

in which U is a general rotation matrix.

In a previous computational study on the photo-induced intramolecular ET dynamics in $[(bpy)_2Ru^{II}(tpphz)Co^{III}(bpy)_2]^{5+}$ this computational protocol was evaluated against quantum dynamical wavepacket simulations, and both methods were found to be in very good agreement.[26] Besides of the application of quantum dynamics[26,30,31,32,33,34] and path integral methods,[35,36] the majority of computational studies addressing ET kinetics are focused on the comparison of the semi-classical Marcus theory and molecular dynamical simulations.[37,38,39,40,41,42,43,44,45]

MOST WIEDZY Downloaded from mostwiedzy.pl

3. Results

3.1 Description of the singlet and triplet excited states properties of $RuPtCl_2$

The properties of the singlet and triplet excited states of $RuPtCl_2$ calculated at the ground state geometry (S_0) were investigated recently.[17] The main results are described here in order to introduce the excited states that are populated upon photoexcitation and that are involved in the ET processes. The MLCT absorption band (Figure 1) in the visible region is mainly obtained from a superposition of eight singlet excited states having non-negligible oscillator strengths (Table 1). Specifically, the low-energy states S_2 and S_9 consist of MLCT transitions to the tpphz bridging ligand (BL), the state S_{16} involves transitions to the bpy ligands, whereas the excited states S_{11}, S_{12}, and S_{15} describe an overlap of MLCT transitions to both the tpphz and bpy ligands. These six states have counterparts in $RuPdCl_2$ (i.e., S_2, S_{13}, S_{15}, S_{16}, S_{17}, and S_{19}), which shows that the initial photoexcitation within the MLCT band is nearly identical in both compounds[13,15,8,1,17]. However, the high-energy part of the MLCT band of $RuPtCl_2$ presents also a contribution from the states S_{18} and S_{19}. These states involve an overlap of MLCT transitions - originating from both metal centers (i.e., $d_{XZ}(Pt) \rightarrow \pi^*_{BL1}$, $d_{XZ}(Ru) \rightarrow \pi^*_{BL3}$) – toward the tpphz ligand, and therefore describe a partial oxidation of the catalytic center ($PtCl_2$). Comparable states (i.e., S_{21}: $d_{XZ}(Ru) \rightarrow \pi^*_{BL3}$, $\lambda = 399$ nm, $f = 0.003$, and S_{28}: $d_{XZ}(Pd) \rightarrow \pi^*_{BL1}$, $\lambda = 370$ nm, $f = 0.266$) are found at higher energy in the case of $RuPdCl_2$, which clearly indicates that the palladium center has a stronger electron accepting character than the platinum center. These modifications in the excited state properties are responsible for the spectral differences observed in the experimental absorption spectra of $RuPdCl_2$ and $RuPtCl_2$ in the 350-400 nm region[8]. A reasonable agreement is found between the simulated absorption maximum of $RuPtCl_2$ in the visible region (2.95 eV) and the experimental value of 2.77 eV (i.e., $\lambda = 448$ nm) in acetonitrile[8]. This is consistent with the results obtained for $RuPdCl_2$ (i.e., Theo.: 2.96 eV, Exp.: 2.79 eV)[1] as well as in general with the typical accuracy expected from TD-DFT calculations on ruthenium complexes (see, e.g., Refs.[46,47,48,49]).

MOST WIEDZY Downloaded from mostwiedzy.pl

Similarly to our previous study on $RuPdCl_2$,[1] the present work assumes an initial photoexcitation of $RuPtCl_2$ around 500 nm. Absorption in this wavelength range will mainly populate the S_2 state (Figure 1) that, as is the case for $RuPdCl_2$, describes a MLCT transition to the tpphz ligand (Table 1) populating the LUMO π^*_{BL1} orbital (Figure 2). For ruthenium complexes, it is established that after the excitation to a singlet excited state, ultrafast ISC occurs due to spin-orbit couplings. Therefore, such ISCs are expected to populate predominantly the energetically close triplet excited states having a similar orbital character as the singlet excited state (i.e., S_2). At the S_0 geometry (Table 1), five triplet excited states have an energy below S_2 (at 2.44 eV), namely the three T_{BL1} states (T_1, T_2, and T_5), which mainly describe MLCT transitions from the three occupied d(Ru) orbitals to the π^*_{BL1} orbital, and the two triplet states T_3 and T_4 (denoted as T_{BL4_YZ} and T_{BL4_XZ}), which consist of an overlap of MLCT transitions to the π^*_{BL4} and π^*_{BL1} orbitals. Additionally, several states relevant to the ET dynamics are reported in Table 1, specifically 1) the four Pt-centered states (T_8, T_{10}, T_{16}, and T_{29}), which involve transitions from the four occupied d(Pt) orbitals to the unoccupied orbital $d^*_{X^2-Y^2}$(Pt), 2) the third T_{BL4} state (T_{14}), 3) the three T_{BL2} (T_{13}, T_{15}, and T_{19}), the three T_{BL3} (T_{22}, T_{27}, and T_{28}) and the three T_{BL5} (T_{42}, T_{52}, and T_{54}) states, and 4) the three charge-separated states T_{CS} (T_{66}, T_{75}, and T_{77}), which describe transitions from the three occupied d(Ru) orbitals to the unoccupied orbital $d^*_{X^2-Y^2}$(Pt). The entire list of the 80 first triplet excited states is reported in the Supporting Information (Table S1 and Figure S1).

In order to estimate the effects of geometrical relaxation on the excited states energies and to investigate ET processes with the semi-classical Marcus theory, geometry optimizations of the five lowest triplet states were attempted using TD-DFT. The optimizations succeeded for the S_2 and for the three T_{BL1} states, whereas no convergence could be achieved for T_{BL4_YZ} and T_{BL4_XZ}. The inability of the calculations to identify equilibrium geometries for these latter states is likely related to the significant overlap between the T_{BL1} and T_{BL4} states. Additionally, successful geometry optimizations were performed for the T_{CS_YZ} and T_{CS_XZ} states, whereas the calculations failed to find a minimum for the T_{CS_XY} state. These states are considered because the population of the T_{CS}

MOST WIEDZY Downloaded from mostwiedzy.pl

states is directly associated to the ET dynamics leading to the desired photoreduction of the catalytic center, which corresponds to the formation of the charge-separated species. Moreover, the geometries of the four T_{Pt} states were optimized because comparable Pd-centered states were found to lead to efficient deactivation channels in $RuPdCl_2$.[1] The geometries of the higher energy T_{BL} states (Table 1) were not optimized, as they are expected to be populated by photoexcitation in the shorter wavelength region of the absorption spectrum ($\lambda < 450$ nm). For the same reason, triplet MLCT states to the bpy ligands and other states corresponding to charge-recombination (Table S1) were not considered.

MOST WIEDZY Downloaded from mostwiedzy.pl

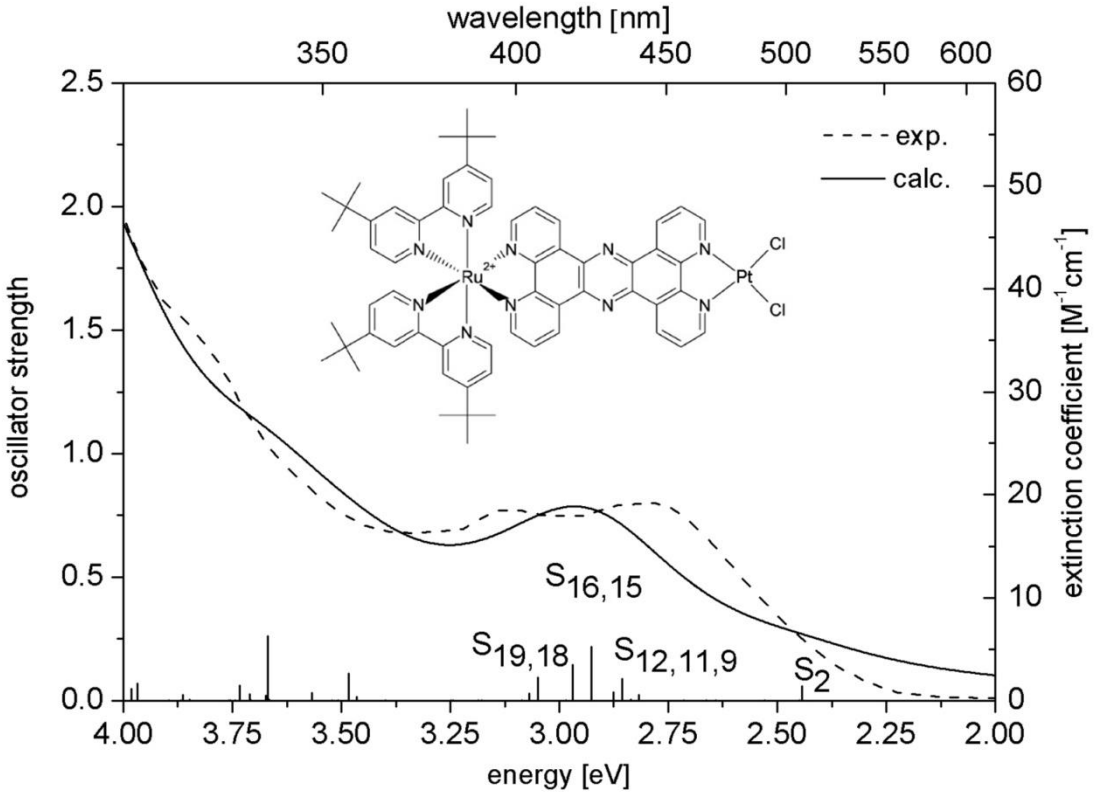

Figure 1. Calculated (black line) and experimental[8] (dashed line) absorption spectra of $RuPtCl_2$. A Lorentzian function with a full width at half maximum (FWHM) of 4000 cm^{-1} is employed to broaden the calculated transitions. The eight main singlet MLCT states are indicated.

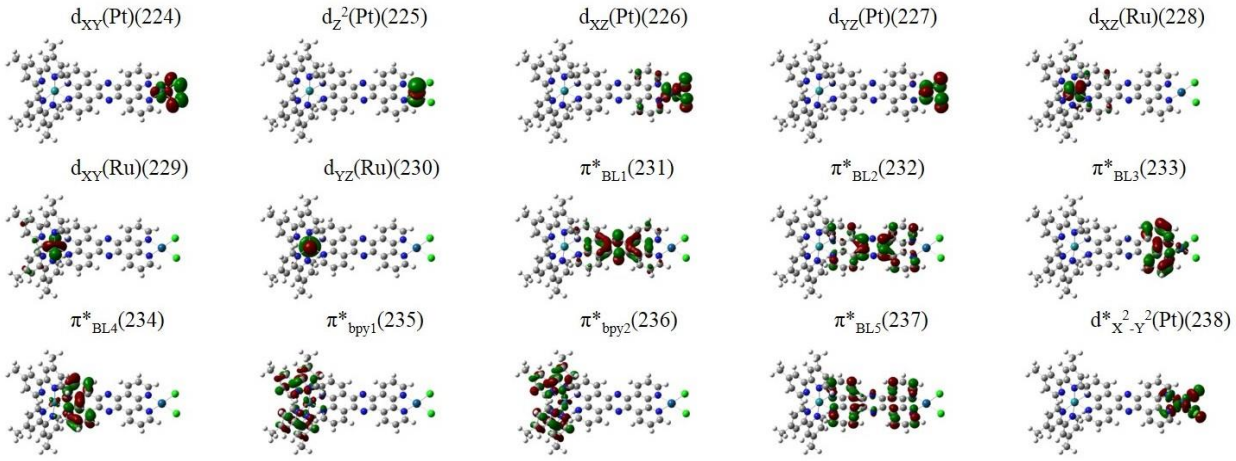

Figure 2. Frontier orbitals of $RuPtCl_2$ and the employed nomenclature including the orbital numbering at the S_0 geometry.

MOST WIEDZY Downloaded from mostwiedzy.pl

Table 1. Vertical excitation energies (VEE), wavelengths (λ), oscillator strengths (f) and singly-excited configurations of the main singlet and triplet excited states calculated at the S_0 geometry for $RuPtCl_2$.

State	Transition	Weight (%)[a]	VEE (eV)	λ (nm)	f
singlet-singlet excitations					
S_2	$d_{XZ}(Ru) \rightarrow \pi^*_{BL1}$	95	2.44	507	0.058
S_9	$d_{XY}(Ru) \rightarrow \pi^*_{BL2}$ $d_{XZ}(Ru) \rightarrow \pi^*_{BL4}$	75 17	2.82	439	0.022
S_{11}	$d_{XZ}(Ru) \rightarrow \pi^*_{BL4}$ $d_{XZ}(Ru) \rightarrow \pi^*_{bpy1}$ $d_{XY}(Ru) \rightarrow \pi^*_{BL2}$	44 39 10	2.86	434	0.088
S_{12}	$d_{XZ}(Ru) \rightarrow \pi^*_{BL2}$ $d_{XY}(Ru) \rightarrow \pi^*_{bpy1}$ $d_{XZ}(Ru) \rightarrow \pi^*_{bpy2}$	46 26 19	2.88	431	0.034
S_{15}	$d_{XY}(Ru) \rightarrow \pi^*_{bpy2}$ $d_{XZ}(Ru) \rightarrow \pi^*_{bpy1}$ $d_{XZ}(Ru) \rightarrow \pi^*_{BL4}$	40 25 19	2.93	423	0.220
S_{16}	$d_{XZ}(Ru) \rightarrow \pi^*_{bpy2}$ $d_{XY}(Ru) \rightarrow \pi^*_{bpy1}$	51 44	2.97	417	0.144
S_{18}	$d_{XZ}(Pt) \rightarrow \pi^*_{BL1}$ $d_{XZ}(Ru) \rightarrow \pi^*_{BL3}$	57 35	3.05	406	0.095
S_{19}	$d_{XZ}(Ru) \rightarrow \pi^*_{BL3}$ $d_{XZ}(Pt) \rightarrow \pi^*_{BL1}$	62 33	3.07	404	0.029
singlet-triplet excitations					
T_1 (T_{BL1_YZ})	$d_{YZ}(Ru) \rightarrow \pi^*_{BL1}$ $d_{YZ}(Ru) \rightarrow \pi^*_{BL4}$	61 26	2.23	556	0.000
T_2 (T_{BL1_XZ})	$d_{XZ}(Ru) \rightarrow \pi^*_{BL1}$ $d_{XZ}(Ru) \rightarrow \pi^*_{BL4}$	58 28	2.36	525	0.000
T_3 (T_{BL4_YZ})	$d_{YZ}(Ru) \rightarrow \pi^*_{BL1}$ $d_{YZ}(Ru) \rightarrow \pi^*_{BL4}$ $d_{YZ}(Ru) \rightarrow \pi^*_{bpy1}$	34 25 10	2.37	522	0.000
T_4 (T_{BL4_XZ})	$d_{XZ}(Ru) \rightarrow \pi^*_{BL1}$ $d_{XZ}(Ru) \rightarrow \pi^*_{BL4}$ $d_{XZ}(Ru) \rightarrow \pi^*_{bpy1}$	33 28 14	2.43	510	0.000
T_5 (T_{BL1_XY})	$d_{XY}(Ru) \rightarrow \pi^*_{BL1}$	77	2.43	509	0.000
T_8 (T_{Pt_YZ})	$d_{YZ}(Pt) \rightarrow d^*_{X^2-Y^2}(Pt)$	65	2.56	484	0.000
T_{10} ($T_{Pt\_Z^2}$)	$d_{Z^2}(Pt) \rightarrow d^*_{X^2-Y^2}(Pt)$	88	2.58	479	0.000
T_{13} (T_{BL2_YZ})	$d_{YZ}(Ru) \rightarrow \pi^*_{BL2}$	78	2.64	470	0.000
T_{14} (T_{BL4_XY})	$d_{XY}(Ru) \rightarrow \pi^*_{BL4}$ $d_{XY}(Ru) \rightarrow \pi^*_{bpy1}$ $d_{XZ}(Ru) \rightarrow \pi^*_{bpy2}$	47 23 17	2.68	462	0.000
T_{15} (T_{BL2_XZ})	$d_{XZ}(Ru) \rightarrow \pi^*_{BL2}$ $d_{YZ}(Pt) \rightarrow \pi^*_{BL3}$	46 16	2.73	453	0.000
T_{16} (T_{Pt_XZ})	$d_{XZ}(Pt) \rightarrow d^*_{X^2-Y^2}(Pt)$	85	2.76	449	0.000
T_{19} (T_{BL2_XY})	$d_{XY}(Ru) \rightarrow \pi^*_{BL2}$	78	2.82	439	0.000
T_{22} (T_{BL3_YZ})	$d_{YZ}(Ru) \rightarrow \pi^*_{BL3}$	59	2.91	425	0.000
T_{27} (T_{BL3_XZ})	$d_{XZ}(Ru) \rightarrow \pi^*_{BL3}$	94	3.06	404	0.000
T_{28} (T_{BL3_XY})	$d_{XY}(Ru) \rightarrow \pi^*_{BL3}$	98	3.07	403	0.000
T_{29} (T_{Pt_XY})	$d_{XY}(Pt) \rightarrow d^*_{X^2-Y^2}(Pt)$	92	3.09	401	0.000
T_{42} (T_{BL5_YZ})	$d_{YZ}(Ru) \rightarrow \pi^*_{BL5}$	79	3.49	355	0.000
T_{52} (T_{BL5_XZ})	$d_{XZ}(Ru) \rightarrow \pi^*_{BL5}$	74	3.63	341	0.000
T_{54} (T_{BL5_XY})	$d_{XY}(Ru) \rightarrow \pi^*_{BL5}$	62	3.67	337	0.000
T_{66} (T_{CS_YZ})	$d_{YZ}(Ru) \rightarrow d^*_{X^2-Y^2}(Pt)$	99	3.87	320	0.000
T_{75} (T_{CS_XZ})	$d_{XZ}(Ru) \rightarrow d^*_{X^2-Y^2}(Pt)$	99	4.02	308	0.000
T_{77} (T_{CS_XY})	$d_{XY}(Ru) \rightarrow d^*_{X^2-Y^2}(Pt)$	99	4.03	307	0.000

[a] Weights larger than 10%.

MOST WIEDZY Downloaded from mostwiedzy.pl

3.2 Electron transfer between T_{BL1} and T_{CS} states in $RuPtCl_2$ and comparison with $RuPdCl_2$

After photoexcitation to S_2, ISC populates most probably the energetically close T_{BL1} states having similar orbital characters as S_2 (Table 1). Figure 3 shows also that the energies of the S_2 and T_{BL1} states remain comparable after relaxation to their geometries. This originates from the similar orbital character of the S_2 and T_{BL1} states, merely differing in the unoccupied d spin-orbital at the ruthenium and in the opposite spin orientation of the singly-occupied π^*_{BL1} orbital. Identical properties of the S_2 and T_{BL1} states were obtained in the case of $RuPdCl_2$.[1] Following population of the T_{BL1} states, the possibility of a direct ET toward the catalytic center (i.e., the T_{CS} states) is investigated. From Figure 3 it is seen that the three T_{CS} states are significantly stabilized, by about 0.5-1.0 eV, when going from the S_0 geometry to the T_{CS} geometries, whereas a destabilization of comparable magnitude occurs for the T_{BL1} states. However, although similar stabilization/destabilization effects lead to an inversion of the energetic positions of the T_{BL1} and T_{CS} states in $RuPdCl_2$,[1] the T_{BL1} states remain below the T_{CS} states in $RuPtCl_2$ at the T_{CS} geometries (Figure 3). This difference is related to the higher energies of the T_{CS} states in $RuPtCl_2$ in comparison to $RuPdCl_2$. For example at the S_0 geometry, the T_{BL1_YZ} state is found at 2.23 eV in both systems, whereas the T_{CS_YZ} state is calculated at 3.02 eV in $RuPdCl_2$[1,17] and at 3.87 eV in $RuPtCl_2$ (Table 1). In general, higher energies (by about 0.8-0.9 eV) are obtained for all the T_{CS} states in $RuPtCl_2$ in comparison to $RuPdCl_2$, this difference is maintained going from the S_0 to the T_{CS} geometries. On the contrary, differences of less than 0.05 eV are found for the T_{BL1} states energies between both systems. This finding is closely related to the spectral changes observed in the experimental absorption spectra in the 350-400 nm region (recall section 3.1), and emphasizes the reduced electron withdrawing nature of the Pt center in comparison to its Pd analogue.

The ET rates from the T_{BL1} to the T_{CS} states are then evaluated by using the semi-classical Marcus theory and are compared with the respective ET rates obtained for $RuPdCl_2$. The two pairs $T_{BL1\_XZ} \rightarrow T_{CS\_XZ}$ and $T_{BL1\_YZ} \rightarrow T_{CS\_YZ}$ are considered, which describe an ET from the π^*_{BL1} orbital to the $d^*_{X^2-Y^2}$(Pt) orbital, assuming that the singly occupied d(Ru) orbital stays unaltered.

MOST WIEDZY Downloaded from mostwiedzy.pl

The diabatic PECs of the donor and acceptor states were calculated with TD-DFT along the coordinate R_{ET} (Figure 4). Due to the high energy of the T_{CS} states, crossings of the PECs are found for values of R_{ET} located on the right side of the T_{CS} minima, i.e., in the inverted region of the reverse ET process ($-\Delta G > \lambda$) in the Marcus picture. The calculated PECs present a nearly parabolic shape, which confirms that the coordinate R_{ET} is adequate for the determination of the ET rates using the Marcus theory. Due to different curvatures of the donor and acceptor PECs, two values of the reorganization energy are obtained (i.e., λ_D and λ_A, see Table 2), consequently two rate constants (k) are estimated for each pair of states. Comparable values of ΔG, λ_D, λ_A and of the maximum potential coupling ($V_{D/A,max}$ obtained at the crossing region) are found for the both $T_{BL1\_XZ} \rightarrow T_{CS\_XZ}$ and $T_{BL1\_YZ} \rightarrow T_{CS\_YZ}$ pairs of states (Table 2). The semi-classical Marcus theory [Eq. (1)] was applied for the computation of the rate constant and of its inverse ($1/k$). The calculated rates are very small with values comprised between 8.68×10^{-8} s^{-1} and 1.89×10^{-7} s^{-1} (Table 2), which is related to the large positive values of the driving force of about 1.15 eV, rendering the ET strongly endergonic. Indeed, $RuPtCl_2$ and $RuPdCl_2$ present comparable values of the reorganization energies and of the maximum potential couplings (see Table 2 and Ref.[1]), whereas the driving forces – entering the exponential function in Eq. (1) – are much smaller for $RuPdCl_2$ with values of about 0.34 eV. This leads to inverse rates of about 10^{14} times larger for $RuPtCl_2$ in comparison to $RuPdCl_2$ (Table 2). Therefore, while the inverse rate constants of about 100 ns for $RuPdCl_2$ describe a slow ET process, the obtained inverse rate constants for $RuPtCl_2$ indicate that a direct $T_{BL1} \rightarrow T_{CS}$ transfer is not possible in this system. This result also implies that the population of the T_{CS} states in $RuPtCl_2$ should involve higher energy T_{BL} states (as e.g., T_{BL3} or T_{BL5}), which could be populated via photoexcitation in the shorter wavelength part of the absorption spectrum, followed by ISC and ET events.

MOST WIEDZY Downloaded from mostwiedzy.pl

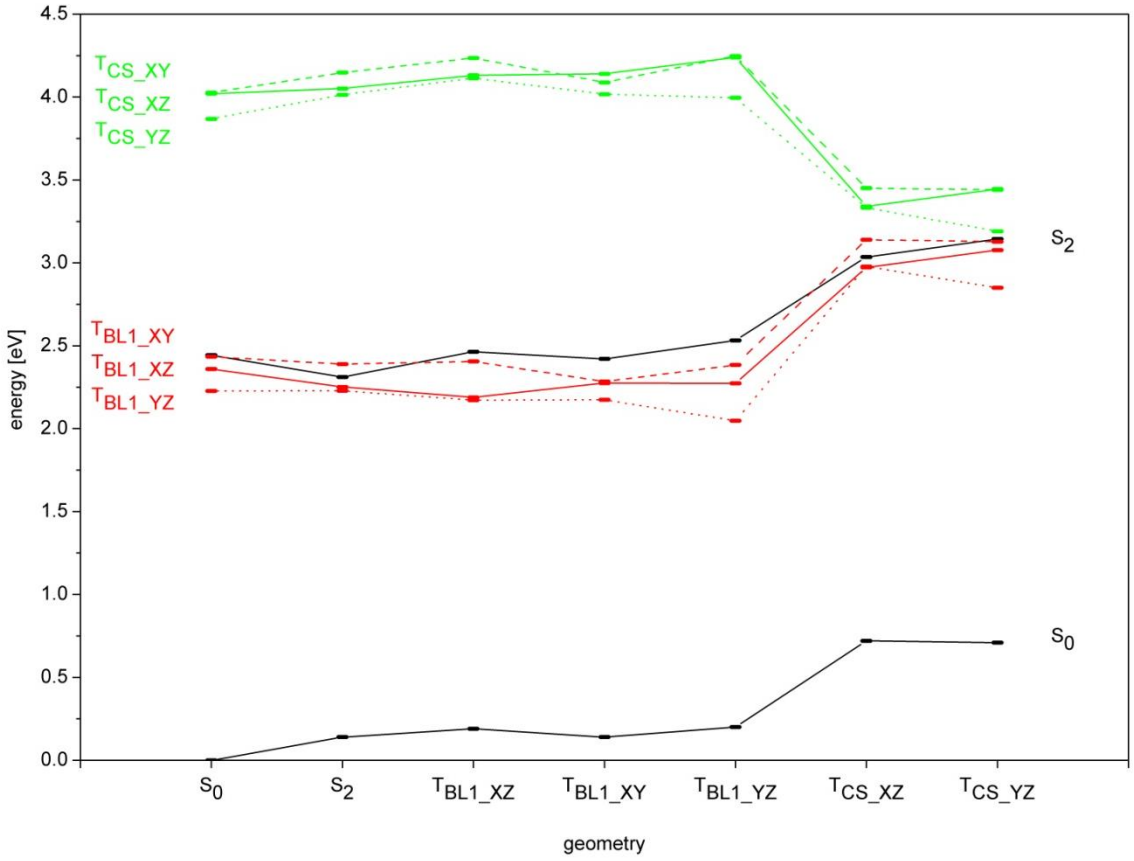

Figure 3. Relative energies of the states of interest at different optimized geometries. Black: the singlet states S_0 and S_2, Red: the three T_{BL1} states, Green: the three T_{CS} states.

Table 2. Driving forces (ΔG), reorganization energies (λ_D and λ_A), potential couplings ($V_{D/A,max}$) and rate constants (k) for pairs of states.

donor → acceptor	$RuPtCl_2$					$RuPdCl_2$[1]	
	ΔG (eV)	λ_i (eV)	$V_{D/A,max}$ (eV)	k_i (s^{-1})	$1/k_i$ (s)	k_i (s^{-1})	$1/k_i$ (s)
$T_{BL1\_XZ} \rightarrow T_{CS\_XZ}$	1.152	0.784	0.034	8.68×10^{-8}	1.15×10^{7}	7.49×10^{6}	1.34×10^{-7}
		0.791		9.32×10^{-8}	1.07×10^{7}	7.68×10^{6}	1.30×10^{-7}
$T_{BL1\_YZ} \rightarrow T_{CS\_YZ}$	1.143	0.802	0.037	1.82×10^{-7}	5.48×10^{6}	1.00×10^{7}	1.00×10^{-7}
		0.805		1.89×10^{-7}	5.29×10^{6}	9.55×10^{6}	1.05×10^{-7}

MOST WIEDZY Downloaded from mostwiedzy.pl

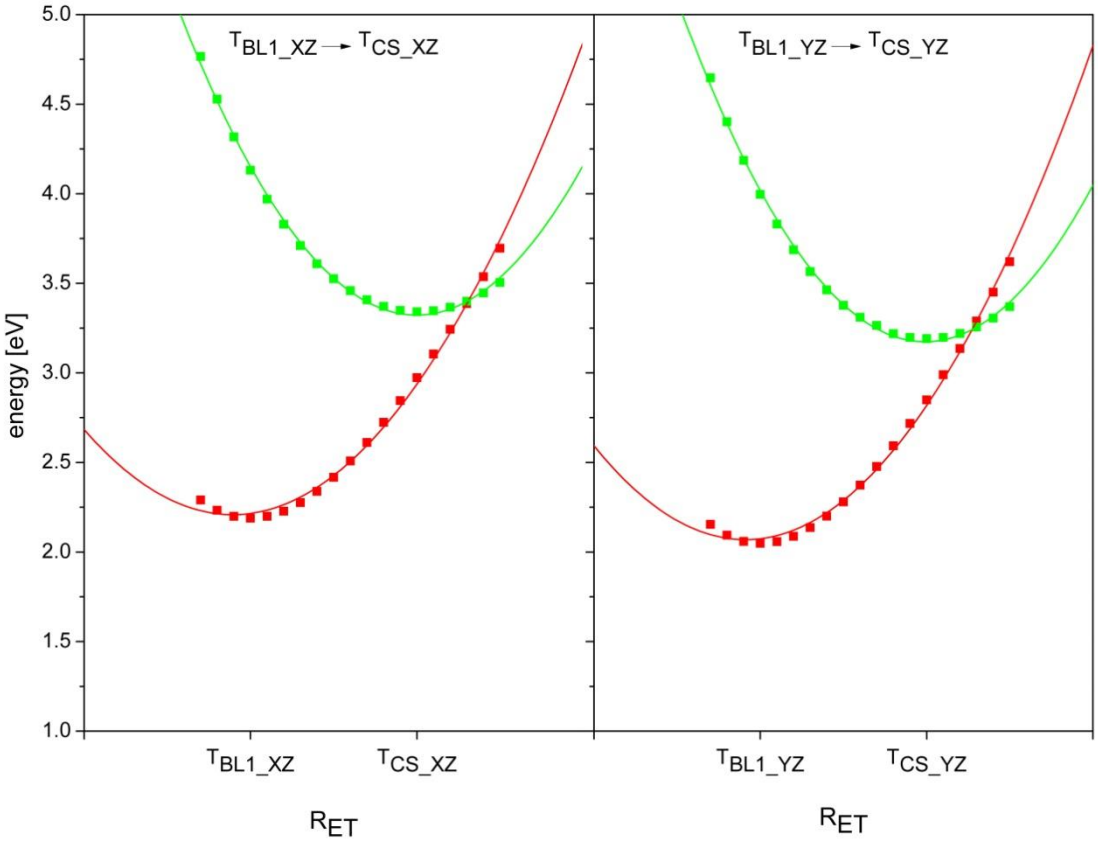

Figure 4. Calculated diabatic PECs of two pairs of donor (T_{BL1}, red squares) and acceptor (T_{CS}, green squares) states obtained at the TD-DFT level of theory along a LICC (R_{ET}). A quadratic polynomial was fitted to the data sets.

3.3 Deactivation processes involving T_{Pt} states in $RuPtCl_2$ and comparison with $RuPdCl_2$

Table 1 shows the presence of four Pt-centered excited states (T_{Pt}) with energies above the T_{BL1} states (Figure 5). T_{Pt} states can be involved in recombination processes through $T_{BL} \rightarrow T_{Pt}$ transfers. Indeed, such a population transfer corresponds to an electron recombination from the bridging ligand toward Ru in conjunction with an energy transfer toward Pt, yielding an excited Pt species. In the case of $RuPdCl_2$, it was found[1] that similar Pd-centered states (T_{Pd}) are very efficiently populated from the T_{BL1} states. Therefore, $T_{BL1} \rightarrow T_{Pt}$ transfers are investigated herein for $RuPtCl_2$. Figure 5 demonstrates that the energies of the T_{Pt} states decrease by about 0.5-1.0 eV between the T_{BL1} and T_{Pt} geometries, whereas the energies of the T_{BL1} states increase by a similar

MOST WIEDZY Downloaded from mostwiedzy.pl

quantity. It is also seen that the T_{Pt} states are well below the T_{BL1} states at the T_{Pt} geometries, which indicates that the $T_{BL1} \rightarrow T_{Pt}$ population transfers are more favorable than charge separation ($T_{BL1} \rightarrow T_{CS}$).

The transfer processes for the twelve pairs of donor (three T_{BL1}) and acceptor (four T_{Pt}) states are considered. For brevity Figure 6 only reports the diabatic PECs involving the T_{BL1_XZ} state, whereas the PECs associated to the T_{BL1_XY} and T_{BL1_YZ} states are given in Figures S2 and S3 of the Supporting Information, respectively. In particular, the PEC of the $T_{Pt\_Z}^2$ state is non-parabolic and possesses a discontinuity at low energies. Similar results were obtained for the $T_{Pd\_Z}^2$ state of $RuPdCl_2$[1], which can be related to the limitations of the (TD)-DFT method for describing significantly distorted geometries. Therefore, the rates were only evaluated for the nine pairs of donor and acceptor states involving the T_{Pt_XY}, T_{Pt_XZ} and T_{Pt_YZ} states (Table 3). The calculated rates cover several orders of magnitude with values comprised between 3.49×10^6 and 1.87×10^{12} s^{-1}. The crossing of the PECs occurs in all cases in the normal region[50] ($|\Delta G| < \lambda$) and the driving forces have either negative values (characterizing an exergonic reaction) or positive values (describing an endergonic reaction). The smallest rate is obtained for the pair $T_{BL1\_YZ} \rightarrow T_{Pt\_XY}$, which involves the lowest T_{BL1} state and the highest T_{Pt} state (ΔG = 0.278 eV). The largest rates are calculated for the pairs $T_{BL1\_XZ} \rightarrow T_{Pt\_YZ}$ and $T_{BL1\_XY} \rightarrow T_{Pt\_YZ}$ with rate constants above 1×10^{12} s^{-1}. It can be noticed that despite having a driving force of ΔG = -0.383 eV, the pair $T_{BL1\_XY} \rightarrow T_{Pt\_YZ}$ has a slightly smaller rate than the pair $T_{BL1\_XZ} \rightarrow T_{Pt\_YZ}$ (ΔG = -0.287 eV). This is due to the smaller potential coupling (0.029 eV) for the pair $T_{BL1\_XY} \rightarrow T_{Pt\_YZ}$. Overall, the inverse rate constants for the $T_{BL1} \rightarrow T_{Pt}$ transfers range from half a picosecond to almost three hundred nanoseconds. This is very different in comparison to $RuPdCl_2$, which presents only exergonic $T_{BL1} \rightarrow T_{Pd}$ reactions having much smaller and less dispersed values of the inverse rate constants comprised between 0.01 and about 2 ps (Table 3).

As mentioned in the introduction, it is known from experimental studies[8,9] that $RuPtCl_2$ is stable during catalysis, whereas $RuPdCl_2$ undergoes an alteration of the catalytic center, which

MOST WIEDZY Downloaded from mostwiedzy.pl

results in the formation of Pd colloids. In the case of $RuPdCl_2$, the fast population of the T_{Pd} states from the T_{BL1} states was proposed to play a key role in the degradation of the Pd-based catalytic center[1]. In particular, it was assumed that the population of T_{Pd} states leads to the dissociation of a Cl^-. This process was justified by the fact that the T_{Pd} states present a decreased bond order of the Pd-Cl bonds due to the singly occupied $d^*_{X^2-Y^2}$(Pd) orbital, thus weakening the Pd-Cl bonds. Indeed, Pd-Cl bond elongations of 0.05, 0.12, 0.11 and 0.19 Å were calculated going from the S_0 geometry to the T_{Pd_XY}, T_{Pd_XZ}, T_{Pd_YZ} and $T_{Pd\_Z^2}$ geometries, respectively[1]. For $RuPtCl_2$, the calculation of the T_{Pt} equilibrium geometries reveals that the Pt-Cl bond length elongations are very similar to $RuPdCl_2$ (Tables S2 and S3 in the Supporting Information). Therefore, these results suggest that the experimentally observed stability of the Pt-based catalytic center does not stem from larger Pt-Cl bond strengths in comparison to the Pd-Cl bonds, but rather originates from differences in the population processes involving the T_{Pt} and T_{Pd} states. Indeed, the differences in the $T_{BL1} \rightarrow T_{Pt}$ and $T_{BL1} \rightarrow T_{Pd}$ rate constants show that - upon excitation of the lowest bright MLCT state (S_2) - the T_{Pt} states are less efficiently populated in $RuPtCl_2$ than the T_{Pd} states in $RuPdCl_2$. Moreover, due to the fact that $T_{BL1} \rightarrow T_{Pt}$ processes of exergonic as well as endergonic nature were obtained, back transfers ($T_{BL1} \leftarrow T_{Pt}$) with comparable magnitude to the $T_{BL1} \rightarrow T_{Pt}$ transfers can occur (i.e., rate constants comprised between 2.12×10^5 and 6.77×10^{11} s^{-1}, see Table S4 in the Supporting Information). On the contrary, $T_{BL1} \leftarrow T_{Pd}$ back transfers are very unlikely in $RuPdCl_2$ with estimated rate constants ranging from 3.22×10^{-4} to 2.50×10^6 s^{-1} (Table S4 in the Supporting Information). This indicates that an equilibrium between the T_{BL1} and T_{Pt} states can occur in $RuPtCl_2$, which might reduce the possibility of Cl^- dissociation, whereas the fast population of the T_{Pd} states in $RuPdCl_2$ and the impossibility of back transfer favor Cl^- loss.

MOST WIEDZY Downloaded from mostwiedzy.pl

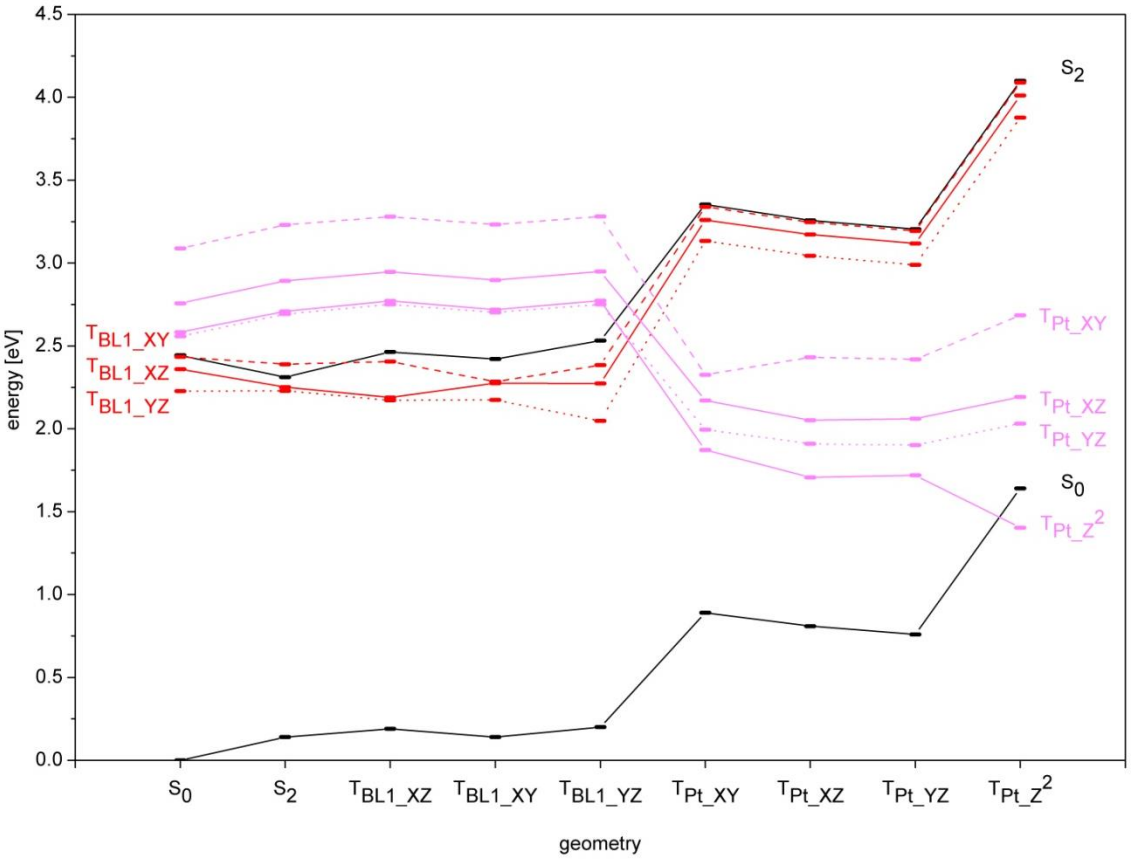

Figure 5. Relative energies of the states of interest at different optimized geometries. Black: the singlet states S_0 and S_2, Red: the three T_{BL1} states, Pink: the four T_{Pt} states.

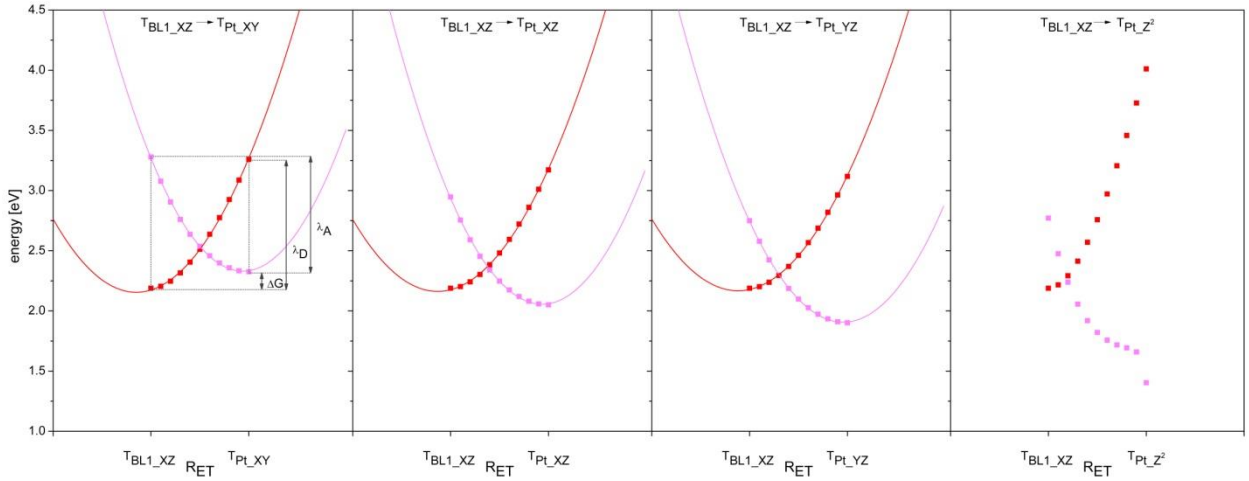

Figure 6. Calculated diabatic PECs of the four pairs of donor (T_{BL1_XZ}, red squares) and acceptor (T_{Pt}, pink squares) states obtained at the TD-DFT level of theory along a LICC (R_{ET}). A quadratic polynomial was fitted to the data sets.

MOST WIEDZY Downloaded from mostwiedzy.pl

Table 3. Driving forces (ΔG), reorganization energies (λ_D and λ_A), potential couplings ($V_{D/A,max}$) and rate constants (k) for pairs of states.

donor → acceptor	$RuPtCl_2$					$RuPdCl_2$[1]	
	ΔG (eV)	λ_i (eV)	$V_{D/A,max}$ (eV)	k_i (s^{-1})	$1/k_i$ (ps)	k_i (s^{-1})	$1/k_i$ (ps)
$T_{BL1\_XZ} \rightarrow T_{Pt/Pd\_XY}$	0.137	1.071 0.954	0.064	1.02×10^{8} 3.33×10^{8}	9800 3010	1.11×10^{13} 1.73×10^{13}	0.0901 0.0578
$T_{BL1\_XZ} \rightarrow T_{Pt/Pd\_XZ}$	-0.138	0.983 0.896	0.068	6.21×10^{10} 1.49×10^{11}	16.1 6.71	7.35×10^{13} 7.75×10^{13}	0.0136 0.0129
$T_{BL1\_XZ} \rightarrow T_{Pt/Pd\_YZ}$	-0.287	0.929 0.849	0.063	8.76×10^{11} 1.87×10^{12}	1.14 0.535	7.95×10^{13} 6.93×10^{13}	0.0126 0.0144
$T_{BL1\_XY} \rightarrow T_{Pt/Pd\_XY}$	0.041	1.055 0.907	0.035	2.77×10^{8} 1.28×10^{9}	3610 781	2.59×10^{13} 4.30×10^{13}	0.0386 0.0233
$T_{BL1\_XY} \rightarrow T_{Pt/Pd\_XZ}$	-0.234	0.962 0.847	0.062	2.88×10^{11} 8.86×10^{11}	3.47 1.13	9.03×10^{12} 7.99×10^{12}	0.111 0.125
$T_{BL1\_XY} \rightarrow T_{Pt/Pd\_YZ}$	-0.383	0.909 0.800	0.029	7.31×10^{11} 1.83×10^{12}	1.37 0.546	9.95×10^{12} 5.21×10^{12}	0.101 0.192
$T_{BL1\_YZ} \rightarrow T_{Pt/Pd\_XY}$	0.278	1.085 0.956	0.067	3.49×10^{6} 1.21×10^{7}	286000 82600	4.37×10^{11} 8.36×10^{11}	2.29 1.20
$T_{BL1\_YZ} \rightarrow T_{Pt/Pd\_XZ}$	0.003	0.996 0.898	0.036	1.16×10^{9} 3.20×10^{9}	860 312	4.08×10^{13} 5.10×10^{13}	0.0245 0.0196
$T_{BL1\_YZ} \rightarrow T_{Pt/Pd\_YZ}$	-0.146	0.941 0.849	0.057	7.57×10^{10} 1.92×10^{11}	13.2 5.21	6.41×10^{13} 7.71×10^{13}	0.0156 0.0130

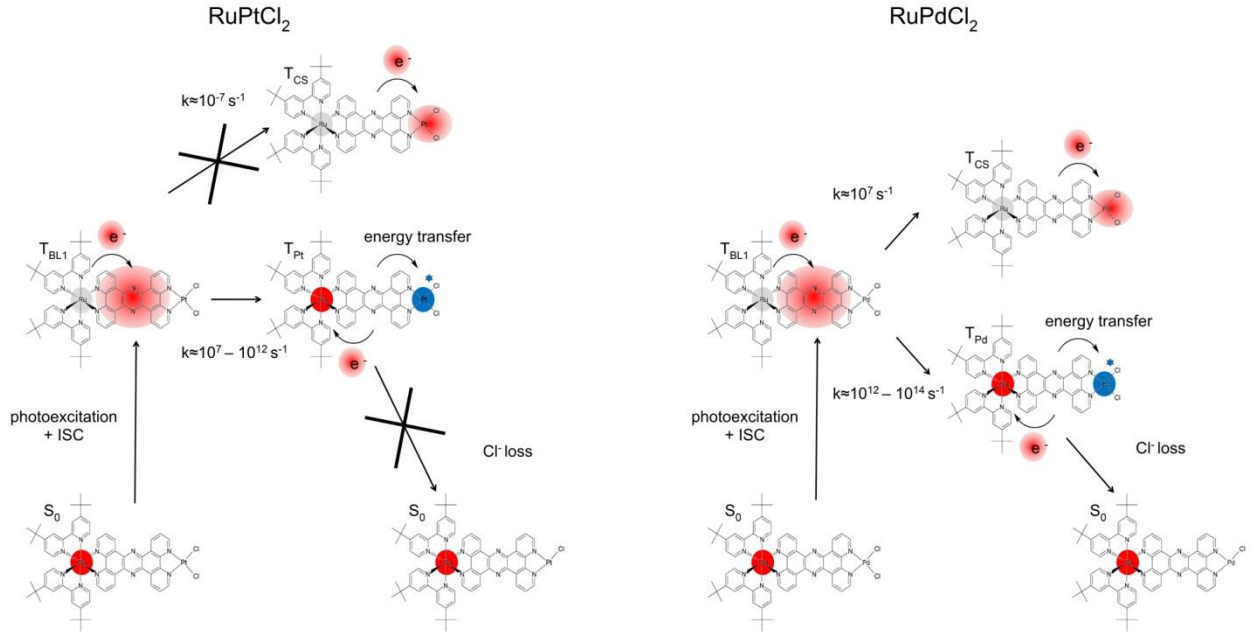

Figure 7. Schematic representation of the theoretically deduced photochemical mechanisms in $RuPtCl_2$ (left) and $RuPdCl_2$ (right).

MOST WIEDZY Downloaded from mostwiedzy.pl

4. Conclusion

The TD-DFT method was used to calculate the energies, orbital characters and excited state geometries of the S_2, T_{BL1}, T_{CS} and T_{Pt} states of $RuPtCl_2$, whereas the semi-classical Marcus theory was employed to determine the ET rates. The obtained results for $RuPtCl_2$ were compared with a previous study[1] on $RuPdCl_2$ in order to assess the impact of the catalytic center on the photochemistry. The simulation of the absorption spectrum shows that the MLCT band of both $RuPtCl_2$ and $RuPdCl_2$ compounds is nearly identical and that an excitation in the longer wavelength range leads predominantly to the population of the S_2 MLCT state. Then, T_{BL1} states are populated by ISC in both photocatalysts (Figure 7).

$T_{BL1} \rightarrow T_{CS}$ transfers have been estimated and rate constants of about 10^{-7} s^{-1} have been obtained for $RuPtCl_2$. The very small values of these rate constants imply that a direct $T_{BL1} \rightarrow T_{CS}$ transfer is not possible in this system. In contrast, the rate constants of $RuPdCl_2$ ($k \approx 10^7$ s^{-1}) are about 10^{14} times larger and describe a slow ET process with inverse rate constant of about 100 ns (Figure 7). The difference in rate constants mainly originates from different values of the driving force, which are associated to the higher energies (by about 0.8-0.9 eV) of the T_{CS} states in $RuPtCl_2$ in comparison to $RuPdCl_2$. Therefore, the population of the T_{CS} states in $RuPtCl_2$ should involve higher energy states (as e.g. T_{BL3} or T_{BL5}), which could be populated via photoexcitation in the shorter wavelength part of the absorption spectrum, followed by ISC and ET events.

The investigation of the $T_{BL1} \rightarrow T_{Pt}$ transfers reveals that these processes are associated to rate constants having a broad range of values, i.e. $k \approx 10^7$-10^{12} s^{-1}. This behavior is due to the energetic proximity of the various T_{BL1} and T_{Pt} states, which leads to both exergonic and endergonic reactions. On the contrary, the $T_{BL1} \rightarrow T_{Pd}$ transfers are significantly faster in $RuPdCl_2$ ($k \approx 10^{12}$-10^{14} s^{-1}) and correspond exclusively to exergonic reactions. The population of the T_{Pt} or T_{Pd} states from the T_{BL1} states acts as a charge recombination process, by re-reducing the ruthenium, and as an energy transfer process toward the catalytic center. As was mentioned[1] in the case of $RuPdCl_2$, the further role of the T_{Pt}/T_{Pd} states can only be speculated. They might promote a relaxation process

MOST WIEDZY Downloaded from mostwiedzy.pl

(by ISC) back to the ground state (S_0) due to their low energies, or they might generate an alteration of the catalytic center by e.g. causing Cl^- loss. In the case of $RuPtCl_2$, $T_{BL1} \leftarrow T_{Pt}$ back transfers are also possible and have comparable rates than $T_{BL1} \rightarrow T_{Pt}$ transfers, which can lead to an equilibrium between the T_{BL1} and T_{Pt} states. Because it is established experimentally[8,9] that $RuPtCl_2$ is stable under catalytic conditions, while $RuPdCl_2$ undergoes an alteration of the catalytic center, it can be proposed that the fast population of the T_{Pd} states and the absence of possible back transfers are responsible for the Cl^- dissociation in $RuPdCl_2$ (Figure 7 and Ref[1]). However, the smaller $T_{BL1} \rightarrow T_{Pt}$ rates and the possibility of an equilibrium between the T_{BL1} and T_{Pt} states might prevent such a Cl^- dissociation, which is expected to provide one element explaining the stability of $RuPtCl_2$. Moreover, these effects induce an increased lifetime of the T_{BL1} states in comparison to $RuPdCl_2$. Such increase might provide e.g. sufficient time for a re-reduction of the ruthenium by the sacrificial electron donor under catalytic conditions. Finally, it is worth mentioning that the high energy of the T_{CS} states in $RuPtCl_2$, which is expected to hinder the formation of the charge-separated state, is in general agreement with its small catalytic turnover number for hydrogen generation (TON = 7)[8], whereas larger TON values were reported[9,19] for $RuPdCl_2$ (TON = 238) as well as for $RuPtI_2$ (TON = 276).

In order to further improve our understanding of the photocatalytic mechanisms in these systems, future studies should address the contribution of higher excited states as well as the second electron transfer processes by considering reduced photocatalysts.

MOST WIEDZY Downloaded from mostwiedzy.pl

Acknowledgments

This work is supported by the Narodowe Centrum Nauki (NCN) (project No. 2014/14/M/ST4/00083). S.K. thanks the Thuringian State Government for financial support within the ACP Explore project. The calculations have been performed at the Universitätsrechenzentrum of the Friedrich-Schiller University of Jena and at the Wrocław Centre for Networking and Supercomputing (grant No. 384). Furthermore, we are grateful for the support of the COST Action CM1202 Perspect-H2O and of the Deutsche Forschungsgemeinshaft (DFG, German Research Foundation) – Projektnummer 364549901 – TRR234 C5.

Supporting Information

Triplet vertical excitation energies, frontier orbitals, diabatic potential energy curves, bond lengths, rate constants for back transfers.

Table of Contents Graphic

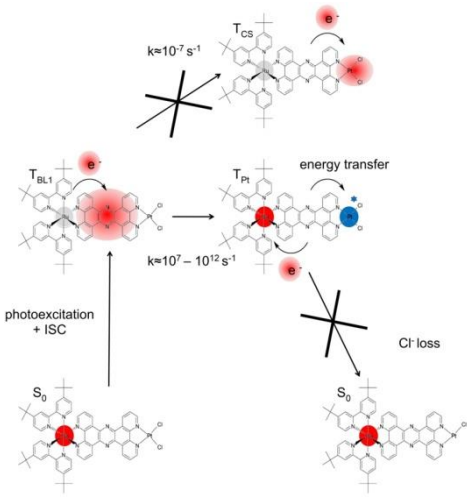

MOST WIEDZY Downloaded from mostwiedzy.pl

References

(1) Staniszewska, M.; Kupfer, S.; Guthmuller, J. Theoretical Investigation of the Electron-Transfer Dynamics and Photodegradation Pathways in a Hydrogen-Evolving Ruthenium-Palladium Photocatalyst. *Chem. Eur. J.* **2018**, *24*, 11166–11176.

(2) Rau, S.; Schäfer, B.; Gleich, D.; Anders, E.; Rudolph, M.; Friedrich, M.; Görls, H.; Henry, W.; Vos, J. G. A Supramolecular Photocatalyst for the Production of Hydrogen and the Selective Hydrogenation of Tolane. *Angew. Chem. Int. Ed.* **2006**, *45*, 6215–6218.

(3) Ozawa, H.; Haga, M. A.; Sakai, K. A Photo-Hydrogen-Evolving Molecular Device Driving Visible-Light-Induced EDTA-Reduction of Water into Molecular Hydrogen. *J. Am. Chem. Soc.* **2006**, *128*, 4926–4927.

(4) Andreiadis, E. S.; Chavarot-Kerlidou, M.; Fontecave, M.; Artero, V. Artificial Photosynthesis: From Molecular Catalysts for Light-Driven Water Splitting to Photoelectrochemical Cells. *Photochem. Photobiol.* **2011**, *87*, 946–964.

(5) Artero, V.; Chavarot-Kerlidou, M.; Fontecave, M. Splitting Water with Cobalt. *Angew. Chem. Int. Ed.* **2011**, *50*, 7238–7266.

(6) Halpin, Y.; Pryce, M. T.; Rau, S.; Dini, D.; Vos, J. G. Recent Progress in the Development of Bimetallic Photocatalysts for Hydrogen Generation. *Dalt. Trans.* **2013**, *42*, 16243–16254.

(7) Hammarström, L. Accumulative Charge Separation for Solar Fuels Production: Coupling Light-Induced Single Electron Transfer to Multielectron Catalysis. *Acc. Chem. Res.* **2015**, *48*, 840–850.

(8) Pfeffer, M. G.; Schäfer, B.; Smolentsev, G.; Uhlig, J.; Nazarenko, E.; Guthmuller, J.; Kuhnt, C.; Wächtler, M.; Dietzek, B.; Sundström, V.; et al. Palladium versus Platinum: The Metal in the Catalytic Center of a Molecular Photocatalyst Determines the Mechanism of the Hydrogen Production with Visible Light. *Angew. Chem. Int. Ed.* **2015**, *54*, 5044–5048.

(9) Pfeffer, M. G.; Kowacs, T.; Wächtler, M.; Guthmuller, J.; Dietzek, B.; Vos, J. G.; Rau, S. Optimization of Hydrogen-Evolving Photochemical Molecular Devices. *Angew. Chem. Int. Ed.* **2015**, *54*, 6627–6631.

(10) Pan, Q.; Freitag, L.; Kowacs, T.; Falgenhauer, J. C.; Korterik, J. P.; Schlettwein, D.; Browne, W. R.; Pryce, M. T.; Rau, S.; González, L.; et al. Peripheral Ligands as Electron Storage Reservoirs and Their Role in Enhancement of Photocatalytic Hydrogen Generation. *Chem. Commun.* **2016**, *52*, 9371–9374.

(11) Tschierlei, S.; Presselt, M.; Kuhnt, C.; Yartsev, A.; Pascher, T.; Sundström, V.; Karnahl, M.; Schwalbe, M.; Schäfer, B.; Rau, S.; et al. Photophysics of an Intramolecular Hydrogen-Evolving Ru–Pd Photocatalyst. *Chem. Eur. J.* **2009**, *15*, 7678–7688.

(12) Tschierlei, S.; Karnahl, M.; Presselt, M.; Dietzek, B.; Guthmuller, J.; González, L.; Schmitt, M.; Rau, S.; Popp, J. Photochemical Fate: The First Step Determines Efficiency of H2 Formation with a Supramolecular Photocatalyst. *Angew. Chem. Int. Ed.* **2010**, *49*, 3981–3984.

(13) Guthmuller, J.; González, L. Simulation of the Resonance Raman Intensities of a Ruthenium-Palladium Photocatalyst by Time Dependent Density Functional Theory. *Phys. Chem. Chem. Phys.* **2010**, *12*, 14812–14821.

(14) Zedler, L.; Guthmuller, J.; Rabelo de Moraes, I.; Kupfer, S.; Krieck, S.; Schmitt, M.; Popp, J.; Rau, S.; Dietzek, B. Resonance-Raman Spectro-Electrochemistry of Intermediates in Molecular Artificial Photosynthesis of Bimetallic Complexes. *Chem. Commun.* **2014**, *50*, 5227–5229.

(15) Wächtler, M.; Guthmuller, J.; Kupfer, S.; Maiuri, M.; Brida, D.; Popp, J.; Rau, S.; Cerullo, G.; Dietzek, B. Ultrafast Intramolecular Relaxation and Wave-Packet Motion in a Ruthenium-Based Supramolecular Photocatalyst. *Chem. Eur. J.* **2015**, *21*, 7668–7674.

(16) Imanbaew, D.; Lang, J.; Gelin, M. F.; Kaufhold, S.; Pfeffer, M. G.; Rau, S.; Riehn, C. Pump-Probe Fragmentation Action Spectroscopy: A Powerful Tool to Unravel Light-Induced

MOST WIEDZY Downloaded from mostwiedzy.pl

Processes in Molecular Photocatalysts. *Angew. Chem. Int. Ed.* **2017**, *56*, 5471–5474.
(17) Martynow, M.; Kupfer, S.; Rau, S.; Guthmuller, J. Excited State Properties of a Series of Molecular Photocatalysts Investigated by Time Dependent Density Functional Theory. *Phys. Chem. Chem. Phys.* **2019**, *21*, 9052–9060.
(18) Pfeffer, M. G.; Zedler, L.; Kupfer, S.; Paul, M.; Schwalbe, M.; Peuntinger, K.; Guldi, D. M.; Guthmuller, J.; Popp, J.; Gräfe, S.; et al. Tuning of Photocatalytic Activity by Creating a Tridentate Coordination Sphere for Palladium. *Dalt. Trans.* **2014**, *43*, 11676–11686.
(19) Karnahl, M.; Kuhnt, C.; Ma, F.; Yartsev, A.; Schmitt, M.; Dietzek, B.; Rau, S.; Popp, J. Tuning of Photocatalytic Hydrogen Production and Photoinduced Intramolecular Electron Transfer Rates by Regioselective Bridging Ligand Substitution. *ChemPhysChem* **2011**, *12*, 2101–2109.
(20) Karnahl, M.; Kuhnt, C.; Heinemann, F. W.; Schmitt, M.; Rau, S.; Popp, J.; Dietzek, B. Synthesis and Photophysics of a Novel Photocatalyst for Hydrogen Production Based on a Tetrapyridoacridine Bridging Ligand. *Chem. Phys.* **2012**, *393*, 65–73.
(21) Frisch, M. J.; Trucks, G. W.; Schlegel, H. B.; Scuseria, G. E.; Robb, M. A.; Cheeseman, J. R.; Scalmani, G.; Barone, V.; Mennucci, B.; Petersson, G. A.; et al. *Gaussian 09, Revision A.02*; Gaussian, Inc., Wallingford CT, 2009.
(22) Becke, A. D. Density-Functional Thermochemistry. III. The Role of Exact Exchange. *J. Chem. Phys.* **1993**, *98*, 5648–5652.
(23) Lee, C.; Yang, W.; Parr, R. G. Development of the Colle-Salvetti Correlation-Energy Formula into a Functional of the Electron Density. *Phys. Rev. B* **1988**, *37*, 785–789.
(24) Andrae, D.; Häußermann, U.; Dolg, M.; Stoll, H.; Preuß, H. Energy-Adjusted Ab Initio Pseudopotentials for the Second and Third Row Transition Elements. *Theor. Chim. Acta* **1990**, *77*, 123–141.
(25) Hariharan, P. C.; Pople, J. A. The Influence of Polarization Functions on Molecular Orbital Hydrogenation Energies. *Theor. Chim. Acta* **1973**, *28*, 213–222.
(26) Koch, A.; Kinzel, D.; Dröge, F.; Gräfe, S.; Kupfer, S. Photochemistry and Electron Transfer Kinetics in a Photocatalyst Model Assessed by Marcus Theory and Quantum Dynamics. *J. Phys. Chem. C* **2017**, *121*, 16066–16078.
(27) Tomasi, J.; Mennucci, B.; Cammi, R. Quantum Mechanical Continuum Solvation Models. *Chem. Rev.* **2005**, *105*, 2999–3093.
(28) Marcus, R. A. On the Theory of Oxidation-Reduction Reactions Involving Electron Transfer. I*. *J. Chem. Phys.* **1956**, *24*, 966–978.
(29) Marcus, R. A. On the Theory of Electron-Transfer Reactions. VI. Unified Treatment for Homogeneous and Electrode Reactions*. *J. Chem. Phys.* **1965**, *43*, 679–701.
(30) Rego, L. G. C.; Batista, V. S. Quantum Dynamics Simulations of Interfacial Electron Transfer in Sensitized TiO2 Semiconductors. *J. Am. Chem. Soc.* **2003**, *125*, 7989–7997.
(31) Borrelli, R.; Di Donato, M.; Peluso, A. Quantum Dynamics of Electron Transfer from Bacteriochlorophyll to Pheophytin in Bacterial Reaction Centers. *J. Chem. Theo. Comput.* **2007**, *3*, 673–680.
(32) Kondov, I.; Cížek, M.; Benesch, C.; Wang, H.; Thoss, M. Quantum Dynamics of Photoinduced Electron-Transfer Reactions in Dye-Semiconductor Systems: First-Principles Description and Application to Coumarin 343-TiO2. *J. Phys. Chem. C* **2007**, *111*, 11970–11981.
(33) Li, J.; Kondov, I.; Wang, H.; Thoss, M. Quantum Dynamical Simulation of Photoinduced Electron Transfer Processes in Dye–Semiconductor Systems: Theory and Application to Coumarin 343 at TiO 2. *J. Phys. Condens. Matter* **2015**, *27*, 134202.
(34) Kupfer, S.; Kinzel, D.; Siegmann, M.; Philipp, J.; Dietzek, B.; Gräfe, S. Fate of Photoexcited Molecular Antennae - Intermolecular Energy Transfer versus Photodegradation Assessed by Quantum Dynamics. *J. Phys. Chem. C* **2018**, *122*, 3273–3285.
(35) Sim, E.; Makri, N. Path Integral Simulation of Charge Transfer Dynamics in Photosynthetic

MOST WIEDZY Downloaded from mostwiedzy.pl

Reaction Centers. *J. Phys. Chem. B* **1997**, *101*, 5446–5458.
(36) Richter, M.; Fingerhut, B. P. Coarse-Grained Representation of the Quasi Adiabatic Propagator Path Integral for the Treatment of Non-Markovian Long-Time Bath Memory. *J. Chem. Phys.* **2017**, *146*, 214101.
(37) Hu, L.; Farrokhnia, M.; Heimdal, J.; Shleev, S.; Rulíšek, L.; Ryde, U. Reorganization Energy for Internal Electron Transfer in Multicopper Oxidases. *J. Phys. Chem. B* **2011**, *115*, 13111–13126.
(38) Blumberger, J. Free Energies for Biological Electron Transfer from QM/MM Calculation: Method, Application and Critical Assessment. *Phys. Chem. Chem. Phys.* **2008**, *10*, 5651–5667.
(39) Oberhofer, H.; Blumberger, J. Charge Constrained Density Functional Molecular Dynamics for Simulation of Condensed Phase Electron Transfer Reactions. *J. Chem. Phys.* **2009**, *131*, 064101.
(40) Menzeleev, A. R.; Ananth, N.; Miller III, T. F. Direct Simulation of Electron Transfer Using Ring Polymer Molecular Dynamics: Comparison with Semiclassical Instanton Theory and Exact Quantum Methods. *J .Chem. Phys.* **2011**, *135*, 074106.
(41) Ungar, L. W.; Scherer, N. F.; Voth, G. A. Classical Molecular Dynamics Simulation of the Photoinduced Electron Transfer Dynamics of Plastocyanin. *Biophys. J.* **1997**, *72*, 5–17.
(42) Kubař, T.; Elstner, M. What Governs the Charge Transfer in DNA? The Role of DNA Conformation and Environment. *J. Phys. Chem. B* **2008**, *112*, 8788–8798.
(43) Hurd, C. A.; Besley, N. A.; Robinson, D. A QM/MM Study of the Nature of the Entatic State in Plastocyanin. *J. Comput. Chem.* **2017**, *38*, 1431–1437.
(44) Tan, M.-L.; Dolan, E. A.; Ichiye, T. Understanding Intramolecular Electron Transfer in Ferredoxin: A Molecular Dynamics Study. *J. Phys. Chem. B* **2004**, *108*, 20435–20441.
(45) Cupellini, L.; Wityk, P.; Mennucci, B.; Rak, J. Photoinduced Electron Transfer in 5-Bromouracil Labeled DNA. A Contrathermodynamic Mechanism Revisited by Electron Transfer Theories. *Phys. Chem. Chem. Phys.* **2019**, *21*, 4387–4393.
(46) Laurent, A. D.; Jacquemin, D. TD-DFT Benchmarks: A Review. *Int. J. Quantum Chem.* **2013**, *113*, 2019–2039.
(47) Daniel, C. Photochemistry and Photophysics of Transition Metal Complexes: Quantum Chemistry. *Coord. Chem. Rev.* **2015**, *282–283*, 19–32.
(48) Jäger, M.; Freitag, L.; González, L. Using Computational Chemistry to Design Ru Photosensitizers with Directional Charge Transfer. *Coord. Chem. Rev.* **2015**, *304–305*, 146–165.
(49) Latouche, C.; Skouteris, D.; Palazzetti, F.; Barone, V. TD-DFT Benchmark on Inorganic Pt(II) and Ir(III) Complexes. *J. Chem. Theory Comput.* **2015**, *11*, 3281–3289.
(50) Marcus, R.; Sutin, N. Electron Transfers in Chemistry and Biology. *Biochim. Biophys. Acta-Reviews Bioenerg.* **1985**, *811*, 265–322.

MOST WIEDZY Downloaded from mostwiedzy.pl